Materials Research Proceedings **32** (2023) 319-329 https://doi.org/10.21741/9781644902615-37

Microstructural and corrosion study of a "non-comercial" high manganese steel

Marcos Natan da Silva Lima[1,3,a], Mauro Andres Cerra Florez[1,b*], Jorge Luiz Cardoso[1,c], João Vitor da Silva Pinto[1], Lucas Moura Farias de Medeiros[1], Walney Silva Araújo[2,d], Hamilton Ferreira Gomes de Abreu[1,e]

[1]Materials Characterization Laboratory (LACAM), Department of Metallurgical and Materials Engineering, Federal University of Ceará, Campus do Pici, bloco 729, Fortaleza 60020-181, Ceará, Brazil

[2]Corrosion Research Laboratory. (LACAM), Department of Metallurgical and Materials Engineering, Federal University of Ceará, Campus do Pici, bloco 729, Fortaleza 60020-181, Ceará, Brazil

[3]Processes for Conformation of Metallic Materials (PROCOMAME), Department Materials Science and Metallurgical Engineering, Universitat Politècnica de Catalunya: Barcelona, Catalunya, Bl. I, 08930, Spain

[a]marcos.natan.da.silva@upc.edu, [b]mauro.cerra@ufc.br, [c]jorgeluizjlc@gmail.com, [d]wsa@ufc.br, [e]hamilton@ufc.br

Keywords: High Mn Steel, Microstructural Characterization, Nacl Corrosion, Hot Rolling, E-Martensite

Abstract. High-Mn steels have great plasticity when subjected to deformation due to TWIP or TRIP effects. This work evaluated the microstructural evolution, the formation of the ε-Martensite phase taking into account the hot rolling of 80-60% and the solution annealing. Afterwards, microstructures were analyzed by SEM. Volume fraction of the Austenite and ε-Martensite phases were measured by EBSD technique. The steel obtained low energy levels of stacking fault, favoring the effect TRIP. Corrosion resistance in 0.1M NaCl solution was analyzed by open potential circuit and potentiodynamic polarization techniques. The analysis of the curves and the surface of the steel after the polarization tests showed that the steel with less strain had relatively nobler potential than the steel with more strain.

Introduction

High manganese steels are called cryogenic steels because they have high mechanical strength and good toughness at temperatures close to that of liquid Nitrogen. In applications at cryogenic temperatures, metals with FCC structure are widely used because they have good mechanical properties at low temperature, while metals with BCC structure show a brittle ductile transition [1]. FeMnC alloys with high levels of Manganese (20-30 wt.%) represent a very recent development of austenitic steels, which, through their differentiated mechanisms of deformation, in TWIP effect (Twinning Induced Plasticity) plastic deformation induced by twins and TRIP (Transformation Induced Plasticity) transformation induced by phase transformation, are of great scientific and economic relevance. Thus a work-scale study following the traditional routes of manufacture of austenitic steels (casting followed by hot mechanical conformation at temperatures above 1000 °C) is necessary, just as it has been practiced by several foreign research groups [2].

Two types of Martensite may occur in austenitic steels. The formation of ε-Martensite, whose crystalline structure is hexagonal compact (HC), and of α'-Martensite, of structure of body-centered cubic or body centered tetragonal (BCC / BCT) [3,4]. The ε-Martensite is still little

Content from this work may be used under the terms of the Creative Commons Attribution 3.0 license. Any further distribution of this work must maintain attribution to the author(s) and the title of the work, journal citation and DOI. Published under license by Materials Research Forum LLC.

explored in austenitic steels. The chemical composition with high manganese content and very low carbon content is very little reported in the literature, mainly by the non-formation of α'-Martensite phase, maintaining the tenacity and ductility properties of the steel. However, the results obtained so far are very promising for the industrial application in very low temperatures of the steel in question. For a research on how the TRIP effect occurs that has the consequence of the formation of ε-Martensite plates is of great relevance. The Stacking Fault Energy (SFE) increases with increasing Mn content, and the TWIP effect is well activated in the SFE range between (18-60 mJ/m^2), thus occurring to the formation of mechanical macros and to values of (SFE < 18 mJ/m^2) the martensitic transformation occurs in the microstructure of the material [4–6]. The ε-Martensite phase also forms at low temperatures in the absence of plastic deformation, whereas for the formation of α'- Martensite a more severe plastic deformation is required. As shown by some authors [5,7–10], the amount of ε-Martensite increases with deformation, reaches a maximum, in larger deformations decreases, while the amount of α'-Martensite increases progressively. Prior to the development of high strength low alloy steels or microalloyed steels (HSLA), carbon and manganese hardened steels thus had poor weldability. The carbon content of the steels produced was around ≅ 0.25%, and today the content has been reduced to around ≅ 0.05%. This reduction substantially improves the weldability of steel [11,12]. That is why the choice of such a low value of carbon in the composition of the steel under study.

In general, the corrosion behavior of high Mn steels in 3.5% NaCl solution is attributed to the high dissolution rate of Mn and Fe atoms in Chloride solutions [13,14]. The formation of unstable oxides in these types of steel allows Mn to be preferably dissolved at the oxide/electrolyte interface. There are some works on the electrochemical polarization behavior of Fe-Mn-Al alloys where some authors have reported that these steels do not passivate in aqueous solutions of 3.5% NaCl, 10% HCl, 0.01M H_2SO_4 or 10% HNO3 and are susceptible to pitting corrosion, but this depends on the alloying elements and their amounts [14-17]. It is also reported that increasing manganese content above 25%, decreases the corrosion resistance of the alloy in aqueous solutions [13-15], as well as adding aluminum to a 25% manganese steel has resulted in increased corrosion resistance in 1M Na_2SO_4, 50% HNO3 and 10-50% NaOH solutions, but this same steel showed no passivation in 10% HCl and 3.5% NaCl solutions [16]. Finally, it is mentioned that as the manganese content in high manganese steels increases, its corrosion resistance decreases [13-18], but the analysis of corrosion in Fe-C-Mn-Si steels is still little reported in the literature, especially for such low carbon values, hence the importance of the current research.

Materials and Methods

Material

The material used in this work was a steel model Fe-Mn-Si-C, manufactured by centrifugal casting, with chemical composition listed in Table 1. Chemical composition obtained in an optical emission spectrometer and compared to that provided by the manufacturer.

Table 1. Chemical composition (wt.%) of the cryogenic steel used in this work.

Mn	C	Si	Ni	Cr	Fe
27	0.027	1.0	0.19	0.41	Bal.

Characterization

The material was manufactured by centrifugal casting, aiming at the reduction of porosities and defects from the casting process. The SFE calculation was produced for the particular program in Microsoft Excel, fitting it to the alloy under study. The quantification of stacking fault energy was

Materials Research Proceedings **32** (2023) 319-329 https://doi.org/10.21741/9781644902615-37

calculated by the proposed thermodynamic mathematical model and used by the author [19] for the Fe-Mn and FeMnC system [20]. The values of free energy, chemical composition, temperature and grain size ASTM of high steel Mn were used. The SFE calculation was carried out using a program specially in Microsoft Excel in order to adapt it to the alloy under study. The samples were hot rolled at 1200 °C, with five passes of the same reduction for deformed samples of 80-60%, with an initial thickness of 9.0 mm. The steel was solution annealed at 1100 °C for 60-90 minutes. After the solution annealing, the steel was cooled in water. After the thermal and mechanical treatments, the samples were prepared for the metallography and polished with alumina. Subsequently, electrolytic polishing was carried out for 20 min, with voltage parameters of 12-15 V and current ranging from 0-2 A. A chemical etching with HNO_3 + H_2O solution was used for a time of 1-5 s. For each condition, several micrographs were obtained in order to analyze the microstructure of Fe-Mn-Si-C steel as received and after deformation/solution annealed. The examined section corresponds to the thickness, plans of the rolling direction, DL. Microstructural analyzes were also carried out on the samples using a scanning electron microscope (SEM) (FE-SEM, Quanta 3D FEG, FEI) used in backscattering electron (BSE) mode. In this same equipment, maps were obtained from the Electron Backscatter Diffraction (EBSD) technique, using the software CHANNEL 5 for the acquisition of maps and quantification of phases. The maps were obtained with an average index of 80% of identified points.

Corrosion test

Corrosion tests were carried out using the Autolab potentiostat/galvanostat PGSTAT 302N controlled by the NOVA® program for data acquisition and treatment. The techniques of open circuit potential (OCP) and potentiodynamic polarization were used in a conventional three-electrode cell at room temperature and in triplicate. The reference electrode used was Ag/AgCl (saturated KCl), the counter electrode was a platinum plate with a rectangular geometrical area of approximately 150 mm^2, and the working electrodes were the samples of Fe27Mn1Si alloy (80-60%) deformed with an area of approximate 30 mm^2. Before the electrochemical measurements, the samples were ground and then washed with deionized water and ethanol. The OCP test was performed for 1 h. Potentiodynamic polarization curves were obtained in a potential range from -50 to +300 mV around the OCP. The scanning rate used was 1 mV/s and the measurements ended when 1 mA current was reached [14,15,17,18]. Due to the potential application of this steel in the construction of cryogenic storage tanks that are commonly located on ships or in areas close to the sea, the NaCl solution was chosen for conducting electrochemical tests. A 0.1M NaCl solution was used and the pH was measured before and after testing. After the corrosion tests, the corrosion products were analyzed with the help of the SEM coupled with an EDS detector.

Results and discussion

Stacking fault energy analysis

The performance fault energy quantification was balanced by the proposed mathematical model and used by Allain et al [21] for the Fe-Mn and FeMnC system. The following free energy components were used: apical temperature, temperature and ASTM grain size of high steel Mn. The addition of alloying elements such as Al and Ni increases SFE and tends to inhibit the martensitic transformation ($\gamma \rightarrow \varepsilon$). The addition of Si decreases SFE, thus favoring ε-Martensite formation during cooling and deformation. The temperature and grain size of the steel also influence the SFE values. The SFE (Γ) in a TRIP / TWIP steel can be estimated using the model proposed by Dumay et al, according to Eq. 1 and Eq. 2.

$$\Gamma = 2\rho\Delta G^{\gamma\rightarrow\varepsilon} + 2\sigma^{\gamma/\varepsilon} \quad (1)$$

$$\Delta G^{\gamma\to\varepsilon} = \Delta G^{\gamma\to\varepsilon}_{FeMnX} + x_c \Delta G^{\gamma\to\varepsilon}_{FeMnX/C} + \Delta G^{\gamma\to\varepsilon}_{mg} \quad (2)$$

The calculated SFE values for Fe-27Mn-1-Si-C steel at cryogenic temperatures (T = -196 ° C) were approximately 5.0 mJ/m^2 and at room temperature of 10.0 mJ/m^2.

Microstructural analysis

Fig. 1 shows the micrographics of the samples 80-60% deformed/solution annealed with water cooling. It can be observed that there was an increase of ε-martensite with water cooling. It is possible to observe the twins from the heat treatment (Annealing Twins) that differ from the twins originated from the high deformation. It is possible to affirm that it is common in some FCC metals (structure of the study material) the presence of twins from the heat treatment.

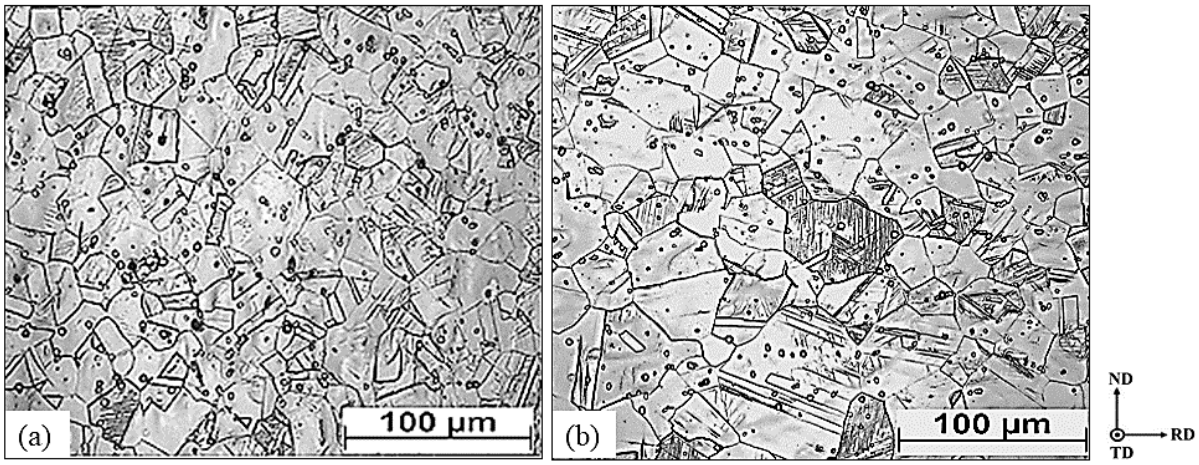

Fig.1. Micrographs of samples deformed with water cooling, 80% deformed (a) and 60% deformed (b).

Unlike the deformation mats, the annealing mats do not occur by shearing, but as irregularities in the growth of deformation-free grains from deformed grains. In the FCC metals, the contour of the blade is from the family (111), and a blade starts when a plan (111) fits the underlying plan in a local configuration of the type HC, rather than the continue FCC configuration.

Still in Fig. 1, microporosities can be observed. When the porosities appear with a white or light green region, it is because the alumina used during the polishing phase in the metallographic preparation covers the micropores. Stains from electrolytic polishing are also observed.

A high grain contour speed (in the fast cooling) favors the formation of annealing mats because the fault of growth in the heat treatment, which are responsible for the formation of mats, are then more frequent. Of course, a low SFE also favors the formation of heat treatment mats (Annealing Twins), since growth fault is easier to achieve [22,23].

After analysis by optical microscopy, grain sizes were calculated for all experimental conditions, as can be observed in Table 2. The method used was the measurement of the intercepts according to ASTM E112 – 13 [24]. The quantification of SFE was calculated by the proposed thermodynamic mathematical model and used by Allain et al [21] for the Fe-Mn and FeMnC system [20]. The values of free energy, chemical composition, temperature and grain size ASTM of high steel Mn were used. The SFE calculation was carried out using a program specially developed in Microsoft Excel, adapting it to the alloy under study.

Materials Research Proceedings **32** (2023) 319-329 https://doi.org/10.21741/9781644902615-37

Table 2. Grain size of the 80-60% deformed / solution annealed rolled samples with water cooling and the stacking fault energy for the Fe27Mn1Si alloy.

Condition	Cooling	Number of intercepts	Grain size (μm)	Error (+/-)
Deformed 80%	Water	183	51	0,2
Deformed 60%	Water	157	63	0.4
SFE (25°) ≅	10 mJ/m^2		-	-
SFE (-196°) ≅	5 mJ/m^2		-	-

In Fig. 2 it is possible to observe in detail the presence of ε-Martensite inside the grains, as well as the absence of it in others. In these cases, it can be explained by the absence of the preferential plan for this metastable phase to occur. There was no shear of the plan (111) - γ for the (100) - ε, for grains without ε-Martensite. In Fig. 2, the microstructure of the 80-60% hot-deformed sample can be observed. Still in Fig. 2, the image of a stunted grain with the presence of ε-Martensite in its interior can be better observed. Oxides can be observed in the sample microstructure, which in turn can be detrimental to the steel properties such as corrosion resistance and mechanical properties.

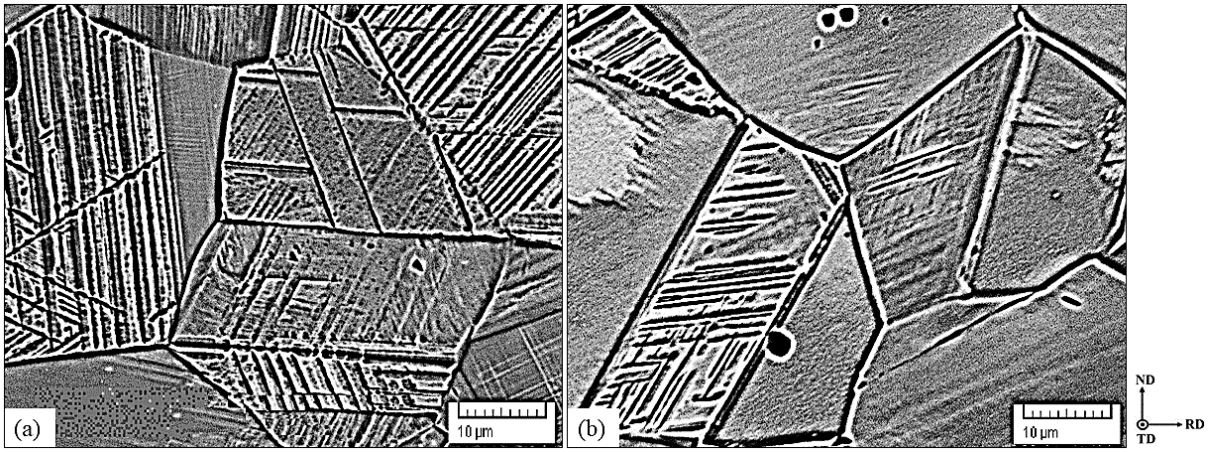

Fig.2. SEM of samples deformed with water cooling, 80% deformed (a) and 60% deformed (b).

The EBSD technique was an important evaluation for the identification and quantification of the phases present in the samples. In addition to the phase identification, it is possible to measure the phase quantity, and also plot the reverse pole figure map (IPF) for the analyzed micro-region, in addition to identify the preferred crystallographic orientation of each phase under study. Fig. 3 shows it that an increase of the martensitic phase occurred. This evidences the appearance of more epsilon martensite, even when the lamination is hot with subsequent cooling in water. For this and other reasons described in the text it is extremely important for research and industry to conduct research on the martensitic transformations of austenitic steels with high levels of Manganese. EBSD maps were also obtained with a high percentage of indexing, increasing the reliability of the technique.

In Fig. 3, one can see the austenitic and martensite grains. In Fig. 3a one can observe the IPF-map. In color, the grains of the austenite phase and in white the ε-martensite phase. In Fig. 3b one can observe the IPF-map, colored for the ε-martensite phase and in white, the grains of austenite phase. In Fig. 3c one can observe the identification of the phases, 90% austenite - and 10% ε-martensite.

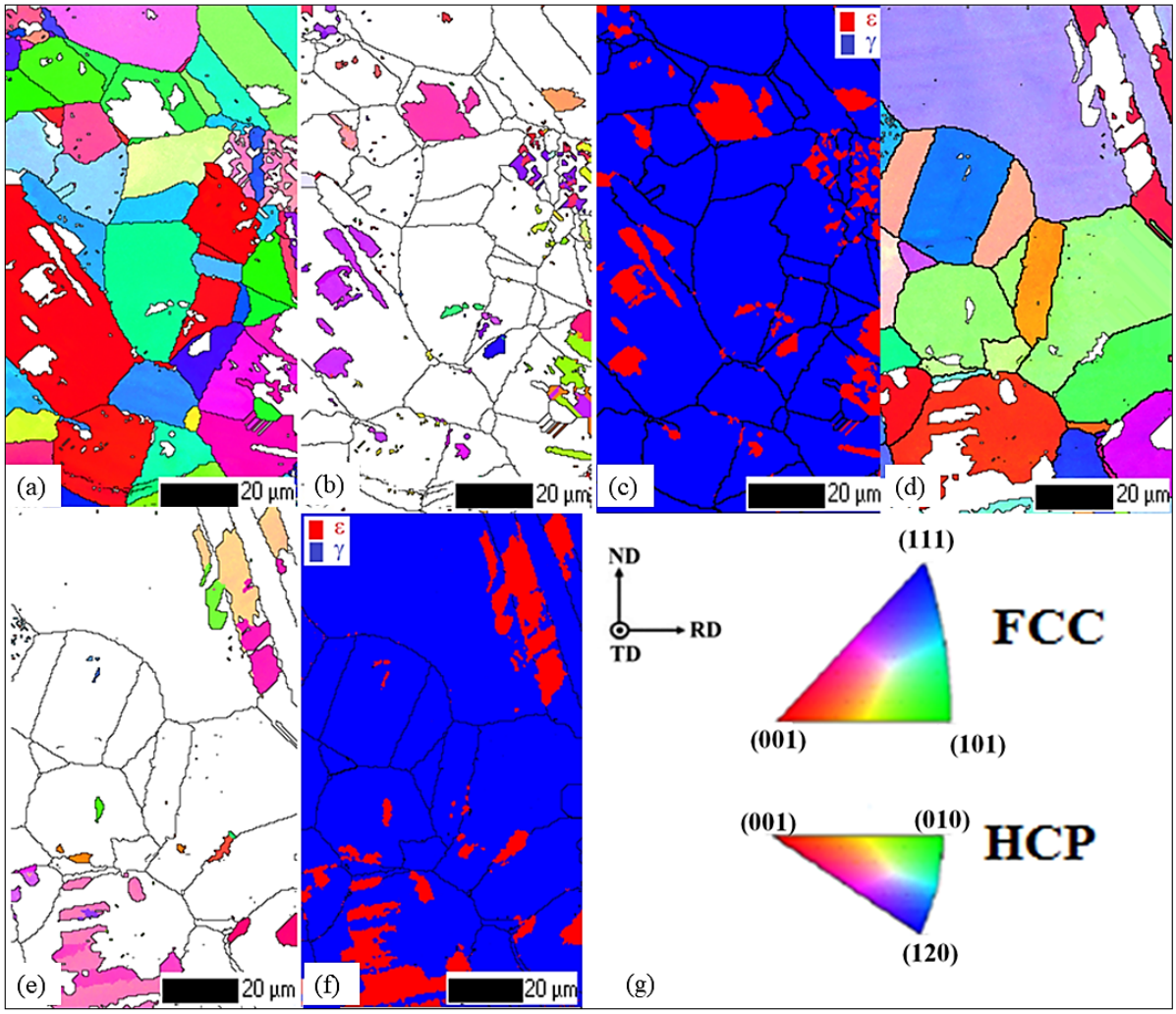

Fig.3. EBSD maps of samples deformed with water cooling. 80% (a) IPF-γ, (b) IPF-ε, (c) phase map, 60% (d) IPF-γ, (e) IPF-ε, (f) phase map, (g) corresponding standard IPF color triangle for γ and ε.

In Fig. 3d, the IPF-γ can be observed, in color the grains of austenite phase and the ε-Martensite phase in white. In Fig. 3e one can observe the map IPF-ε, in color the ε-Martensite phase and in white the grains of the austenite phase. In Fig. 3f one can observe the identification of phases, 89% austenite-γ and 11% ε-Martensite.

Corrosion analysis

The variation of OCP as a function of time for the two Mn high steel conditions evaluated in 0.1 M NaCl solution is shown in Fig. 4a. The curve presented for each condition of Fe27Mn1Si alloy was chosen as the most representative of the triplicate tests performed of each thermomechanical treatment condition in which the alloy was subjected. Fig. 4a shows that the steel with 60% deformation had slightly more noble behavior than the deformed 80% one. Although the values of OCP potentials are close, it is important to remember that it is the same steel, and that the difference in deformation could influence the electrochemical behavior, due to the TWIP phenomenon, more grain limits on the surface of the steel bring a greater area reactive susceptible to corrosion [14,15].

The 60% deformed sample had a decrease in potential in the first minutes of the test, and had variations until stabilized in 2000 s. Similarly, 80% deformed steel had variations with the difference that this steel was able to stabilize faster. This variation in potential is due to

electrochemical interactions between the surface of the sample and the solution, that is, the formation of the double electrochemical layer until the steady state equilibrium is found [14,15].

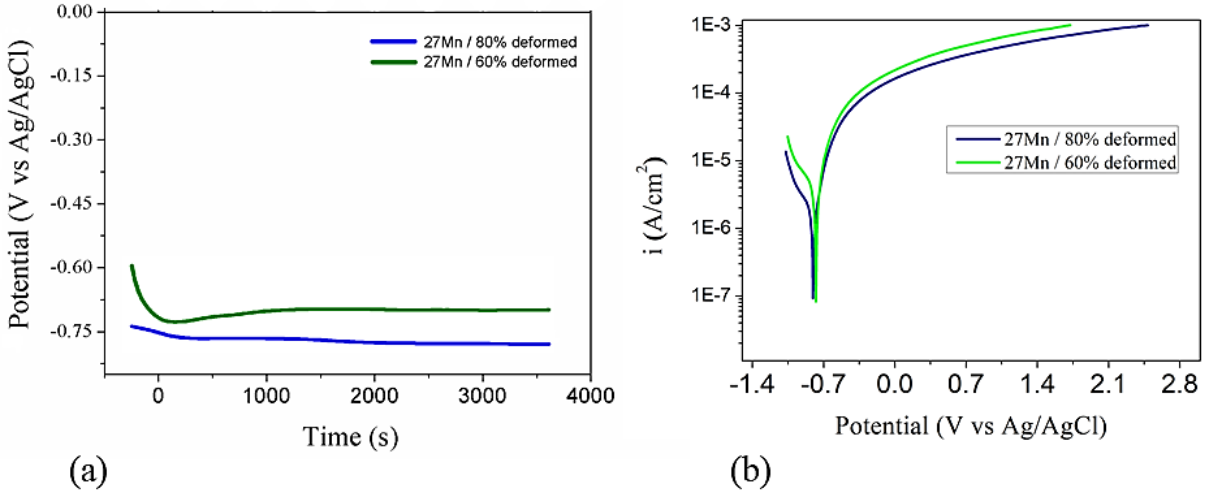

Fig.4. OCP (a) and anodic polarization curves (b) of samples deformed with water cooling (80-60%) deformed in 0.1M NaCl solution.

Fig. 4b shows the potentiodynamic polarization curves in 0.1 M NaCl solution for each Fe27Mn1Si alloy condition (80% and 60% deformed). It can be observed that high Mn steels do not exhibit passivating behavior. This is indicative of the low corrosion resistance of these steels in this medium, as also mentioned by Hyung et al [14-16]. Polarization curves show that the steels behaved similarly in both cathodic and anodic branches. There are slight variations in the current in the cathodic branch, but it is generally identified that the reaction is diffusion-controlled [14,15,25,27].

In the anodic branch, the behavior between them was similar, active dissolution of the material, as presented by Cerra et al [14,15]. More evident variations were found in the corrosion current (i_{corr}), it is possible to observe in the graph a lower corrosion rate in the deformed steel 60%. After the analysis with the Taffel curves, it was possible to obtain the icorr values, indicated in Table 3; these values confirm the less noble character of steel with 80% deformation. These differences found could be associated with the applied deformation (TWIP and TRIP effects) depending on the fact that it is the same steel (with the same chemical composition).

In our understanding, the differences in the results both in OCP and in the polarization tests could be associated with the deformation employed, thus, with the increased deformation, the corrosion resistance can decreases. This reasoning are due to the larger amount of grain boundaries per area (TWIP effect), to the amount of porosity and the greater presence of ε-martensite which contribute to higher surface reactivity and a faster surface oxidation [14,15,27,28], this was confirmed with the corrosion potential (icorr) shown in Table 3, showing a slightly less active surface (60% deformed steel) compared to 80% deformed steel.

Table 3. *Corrosion Potentials (Ecorr) of Fe27Mn1Si (80-60%) deformed in 0.1M NaCl solution.*

Corrosion parameters of the Fe27Mn1Si alloy		
	80% Deformed	60% Deformed
Ecorr (V)	-0.744	-0.776
Icorr (A/cm^2)	3.3E-5	1.8E-5

Materials Research Proceedings **32** (2023) 319-329 https://doi.org/10.21741/9781644902615-37

The measured pH of the 0.1 M NaCl solution before and after the tests was close to seven. The pH value of 7.0 was used to study and analyze the Pourbaix diagrams of the alloying elements of this steel. With the pH and the measured potentials, it was found that in steels with high manganese content, the elements Mn and Fe have a greater tendency to pass to solution as ions than to remain in the metal matrix, besides forming non-protective oxides on the surface in aqueous solutions [13-15,17,25,26,29].

In Fig. 5a, one can see an image obtained by SEM of the 80% deformed high manganese steel sample after potentiodynamic polarization tests. A layer of corrosion products can be observed across the sample surface.

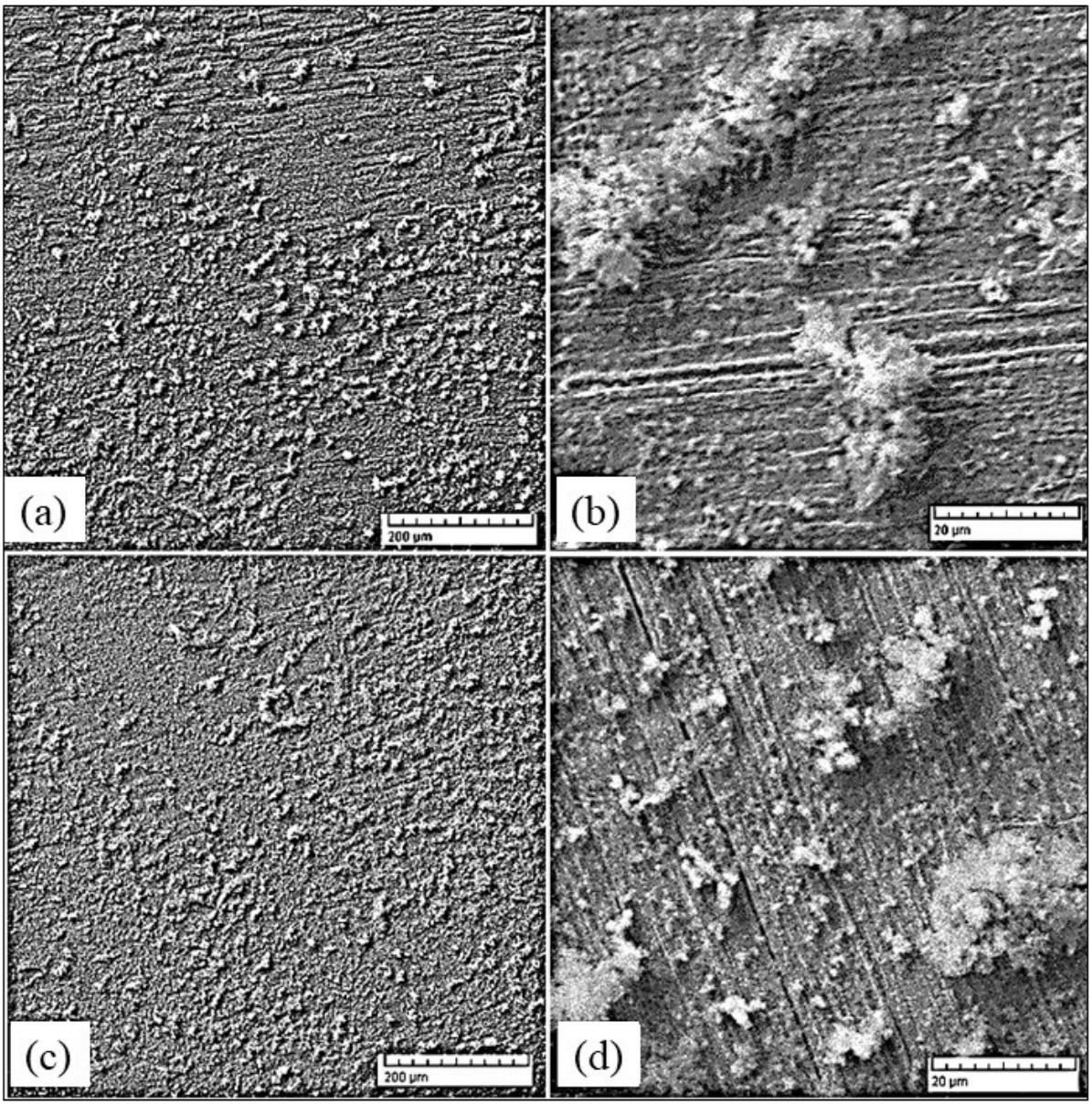

Fig.5. SEM of corrosion products in 0.1M aqueous NaCl solution of samples deformed with water cooling 80% deformed (a) and (b), 60% deformed (c) and (d).

In Fig. 5b, one can see an image obtained in SEM, where it is possible to identify the layer of corrosion products formed on the surface. These corrosion products (normally formed by the oxides γ-FeOOH (lepidocrocite) and α-FeOOH (goethite)) pass directly to the electrolyte, and this was observed by the yellow color (green rust) of the solution after the test as described by Reza et

al [26] and Cerra et al [14,15]. Still in Table 4, it can observe the result of the EDS punctual measurement of the corrosion products of high manganese steel for the conditions studied in this work. The composition was observed through the peaks of the elements Fe, Mn, Si and O (It is essential to indicate that oxygen was only taken into account for comparative purposes). Fig. 5c shows an image obtained by SEM of the sample of high manganese steel, after the potentiodynamic polarization tests. Corrosion products may be observed on the sample surface. Fig. 5d shows the corrosion products and the sanding marks in more detail. Comparing with the previous condition, a layer of corrosion products on the surface was also formed, and dissolved in the electrolyte, which was verified by the yellowish coloration of the solution after the polarization test. In Fig. 5d, one can see the result of the EDS spot measurement of $Fe_{27}MnSi$ alloy corrosion products.

Table 4. EDS of corrosion products in 0.1M solution of Fe27Mn1Si NaCl, 80% deformed and 60% deformed, respectively.

Elements	C Norm. [%wt] (80% def)	C Norm. [%wt] (60% def)
O	31.12	29.32
Si	1.45	1.38
Mn	13.20	13.58
Fe	54.23	55.72

Table 4 shows the quantification of the measurement for the elements made in the EDS analysis of the corrosion products mentioned above. Analyzing the EDS results made in the corrosion products, it was found that the layer contains iron, manganese, silicon and oxygen, which indicates that there are mainly oxides of these elements, as mentioned by Cerra et al [14,15].

Small peaks of the elements manganese and silicon were found, which also form oxides on the sample surface. It is important to mention that unlike Ni and Cr alloys, as mentioned earlier, the high manganese content negatively influences corrosion resistance. Manganese tends to pass into the solution as ions, leaving spaces in the matrix that are used by the electrolyte to corrode the steel [13-15,17,26,28].

Conclusions

Based on the experimental results obtained, it is possible to conclude that the FeMnSi steel presents well-activated transformation mechanisms (Austenite-γ → ε-Martensite), TRIP effect. The microstructure of the FeMnSi steel showed austenitic grains, microporosities from the smelting process. It also presented heat treatment twins, difference in grain size and percentage of phase before and after processing. The ε-martensite phase was found in greater proportions after deformation and heat treatment with cooling in water. It is possible to observe the nucleated martensitic phase within the grains due to the shear planes. This shear is due to the low stack failure energy and the thermal and mechanical stresses to which the alloy was subjected.

The phase transformation occurs from the shear of the FCC => HC structure planes and the high displacement density. Regarding the corrosion resistance of the high manganese steel under study, it did not show passivation due to the large amount of Mn in its composition, which in aqueous solutions, this element has an affinity to leave the metallic matrix and pass as ions, in addition to forming non-protective oxides on the surface of the metal sample.

The deformation of the steels influenced the reduction of the corrosion potential, due to the greater amount of grain contours per area, the amount of micropores and the greater presence of ε-martensite produced during the mechanical process.

The corrosion products formed on the surfaces of high manganese steels do not offer protection due to the presence of undesirable phases and high porosity, which allows electrolyte ions to reach the metal surface, accelerating the corrosion process of the steel.

Acknowledgments
The authors would like to thank Funcap (Cearense Foundation to Support Scientific and Technological Development) for the financial support for this research. The authors would like to thank the Central Analítica-UFC (funded by Finep-CT-INFRA, CAPES-Pró-Equipamentos, and MCTI-CNPq-SisNano2.0) for microscopy measurements, the LACAM-UFC and LPC-UFC Research Groups for technical support.

Declaration of competing interest
This work has no competing of interests or personal relationships that can influence it.

References

[1] Marquardt ED, Le JP, Radebaugh R. Cryogenic material properties database, in: Cryocoolers 11, Springer, 2002:681-687. https://doi.org/10.1007/0-306-47112-4_84

[2] Mi Z, Tang D, Jiang H, Dai Y, Li S. Effects of annealing temperature on the microstructure and properties of the 25Mn-3Si-3Al TWIP steel, Int J Miner. Metall Mater. 2009; 16:154-158. https://doi.org/10.1016/S1674-4799(09)60026-1

[3] Dafé SSF, Sicupira FL, Matos FCS, Cruz NS, Moreira DR, Santos DB. Effect of cooling rate on (ε, α') martensite formation in twinning/transformation-induced plasticity Fe-17Mn-0.06 C steel, Mater Res 2013; 16:1229-1236. https://doi.org/10.1590/S1516-14392013005000129

[4] Talonen J, Hänninen H, Nenonen P, Pape G. Effect of strain rate on the strain-induced γ→ α′-martensite transformation and mechanical properties of austenitic stainless steels, Metall Mater Trans. A. 2005;36: 421-432. https://doi.org/10.1007/s11661-005-0313-y

[5] Hamada AS, Karjalainen LP, Somani MC. The influence of aluminum on hot deformation behavior and tensile properties of high-Mn TWIP steels, Mater Sci Eng. A. 2007; 467:114-124. https://doi.org/10.1016/j.msea.2007.02.074

[6] Jung JE, Park J, Kim JS, Jeon JB, Kim SK, Chang YW. Temperature effect on twin formation kinetics and deformation behavior of Fe-18Mn-0.6 C TWIP steel, Met Mater Int. 2014;20: 27-34. https://doi.org/10.1007/s12540-014-1008-y

[7] Cina B. A transitional hcp phase in the γ→ α transformation in certain Fe-base alloys, Acta Metall. 1958; 6:748-762. https://doi.org/10.1016/0001-6160(58)90050-6

[8] B. Cina, Effect of cold work on the gamma-alpha transformation in some Fe-Ni-Cr alloys, J Iron Steel Inst. 1954; 177:406.

[9] Cullity BD, Stock SR. Elements of X-ray Diffraction, Prentice hall New Jersey, 2001.

[10] Pardal JM, Tavares SSM, Fonseca MPC, da Silva M.R, Neto JM, Abreu HFG. Influence of temperature and aging time on hardness and magnetic properties of the maraging steel grade 300, J Mater Sci. 2007; 42:2276-2281. https://doi.org/10.1007/s10853-006-1317-8

[11] Gorni A, da Silveira JD. Accelerated cooling of steel plates: the time has come, in: Quenching Cool. Residual Stress Distortion Control, ASTM International, 2010.

[12] Bai Y, Bai Q. Subsea pipelines and risers, Elsevier, 2005.

[13] Zhang YS, Zhu XM, Liu M, Che RX. Effects of anodic passivation on the constitution, stability and resistance to corrosion of passive film formed on an Fe-24Mn-4Al-5Cr alloy, Appl Surf. Sci. 2004; 222: 89-101. https://doi.org/10.1016/j.apsusc.2003.08.068

[14] Florez M.A.C., Lima, M. N. D. S., Araújo, W. S., & Silva, M. J. G. D. Characterization and Comparative Analysis of Corrosion Resistance of 4 High Manganese Steels Models in Aqueous Solution of NaCl. Mater Res. 2019, 22. https://doi.org/10.1590/1980-5373-mr-2019-0283

[15] Cerra Florez, M. A., Cardoso, J. L., Ferreira Gomes de Abreu, H., Araújo, W. S., & Gomes da Silva, M. J. Comparative study of corrosion resistance between four non-commercial high manganese steel models and 9% nickel steel in aqueous solution of H2SO4. Int J Mater Res, 2020, 111(8), 661-667. https://doi.org/10.3139/146.111925

[16] H.S. Seo, J.H. Park, J.Y. Park, J.G. Choi, J.K. Kim. Presented at Twenty-Fourth Int. Ocean Polar Eng. Conf., International Society of Offshore and Polar Engineers, 2014.

[17] Hamada AS, Karjalainen LP. Corrosion Behaviour of High-Mn TWIP Steels with Electroless Ni-P Coating, Open Corros. J. 2010;3:1-6. https://doi.org/10.2174/1876503301003010001

[18] Aperador WA, Ruiz JHB, Betancurt JD. Evaluation of erosion-corrosion resistance in Fe-Mn-Al austenitic steels, Mater Res. 2013;16:447-452. https://doi.org/10.1590/S1516-14392012005000179

[19] ASTM, Standard test methods and definitions for mechanical testing of steel products, ASTM A370. 2012.

[20] Dumay A, Chateau JP, Allain S, Migot S, Bouaziz O. Influence of addition elements on the stacking-fault energy and mechanical properties of an austenitic Fe-Mn-C steel, Mater Sci Eng A. 2008;483:184-187. https://doi.org/10.1016/j.msea.2006.12.170

[21] Allain S, Chateau JP, Bouaziz O, Migot S, Guelton N. Correlations between the calculated stacking fault energy and the plasticity mechanisms in Fe-Mn-C alloys, Mater Sci Eng A. 2004; 387:158-162. https://doi.org/10.1016/j.msea.2004.01.059

[22] Callister Jr WD, Rethwisch DG. Fundamentals of materials science and engineering: an integrated approach, John Wiley & Sons, 2012.

[23] Rath BB, Imam MA, Pande CS. Nucleation and growth of twin interfaces in FCC metals and alloys, Mater Phys Mech. 2000;1: 61-66.

[24] A. Standard, E112-13. Standard test methods for determining average grain size, ASTM International, West Conshohocken, (n.d.).2013.

[25] Opiela M, Grajcar A, Krukiewicz W. Corrosion behaviour of Fe-Mn-Si-Al austenitic steel in chloride solution, J Achiev Mater Manuf Eng.2009;33: 159-165.

[26] Razavi GR, Gholami H, Zirepour GR, Zamani D, Saboktakin M, Monajati H. Study corrosion of high-Mn steels with Mo in 3.5% NaCl solution, Conf Adv Mater Eng. IPCSIT, 2011. https://doi.org/10.4028/scientific5/AMR.457-458.334

[27] Lasek S, Mazancová E. Influence of thermal treatment on structure and corrosion properties of high manganese triplex steels, Metalurgija. 2013;52:441-444.

[28] Grajcar A, Kciuk M, Topolska S, Płachcińska A, Microstructure and corrosion behavior of hot-deformed and cold-strained high-Mn steels, J Mater Eng Perform.2016; 25: 2245-2254. https://doi.org/10.1007/s11665-016-2085-5

[29] Fajardo S, Llorente I, Jiménez JA, Bastidas JM, Bastidas DM. Effect of Mn additions on the corrosion behaviour of TWIP Fe-Mn-Al-Si austenitic steel in chloride solution, Corros Sci. 2019;154: 246-253. https://doi.org/10.1016/j.corsci.2019.04.026